Advanced Performance Materials 6, 5–31 (1999)
© 1999 Kluwer Academic Publishers. Manufactured in The Netherlands.

An Overview of Hydrogen Interaction with Amorphous Alloys

N. ELIAZ AND D. ELIEZER
Department of Materials Engineering, Ben-Gurion University of the Negev, Beer-Sheva 84105, Israel

Abstract. Theories, experimental results and applications associated with hydrogen behavior in amorphous metals and alloys are reviewed. An emphasis is made on the potential use of these advanced materials for hydrogen storage technology. Therefore, several properties that are especially relevant for such applications are assessed. These include structural models for hydrogen occupancy, sorption characteristics, solubility, diffusion behavior and thermal stabilities. Hydrogen effects on the mechanical properties and fracture modes of glassy metals are also presented, and possible mechanisms of hydrogen embrittlement are discussed. Similarities and differences between hydrogen behavior in amorphous and crystalline metals and alloys are discussed in detail.

Keywords: amorphous, hydrogen diffusivity, hydrogen embrittlement, hydrogen storage, metallic glasses

1. Introduction

Amorphous metals and alloys can be produced [1–5] by various techniques, such as: rapid quenching of a melt, thermal evaporation, sputtering, electrodeposition and ion implantation. In all these methods, samples are usually obtained in the form of thin film or ribbon. Amorphous alloys can also be fabricated by mechanical alloying, or in some cases by simply hydrogenating the crystalline alloys, to obtain powder samples.

The interaction of hydrogen with amorphous metals has been studied extensively during the last two decades. These studies were motivated by both scientific and technological interests, mainly the potential use of amorphous hydrides in hydrogen storage technology. Many papers dealing with specific systems [6–10] as well as some reviews [11–17] have already been published on this subject.

The present paper is aimed to summarize our recent progress and to review our current understanding of hydrogen interaction with amorphous metals and alloys. Various aspects of this subject, including structural models for hydrogen occupancy, absorption/desorption characteristics, hydrogen diffusivity and solubility, hydrogen effects on the thermal stability, and possible mechanisms of hydrogen embrittlement in amorphous materials, are reviewed. Hydrogen-induced amorphization, however, will be reviewed in detail elsewhere [18]. In addition to analytical discussions, an attempt is made to identify topics that warrant further research and to describe potential applications of hydrogen in amorphous metals and alloys.

2. Structural models for hydrogen occupancy

Various structural models [19–29] have been suggested in order to explain hydrogen absorption and diffusion in amorphous alloys. Kirchheim et al. [19–22] propose that since

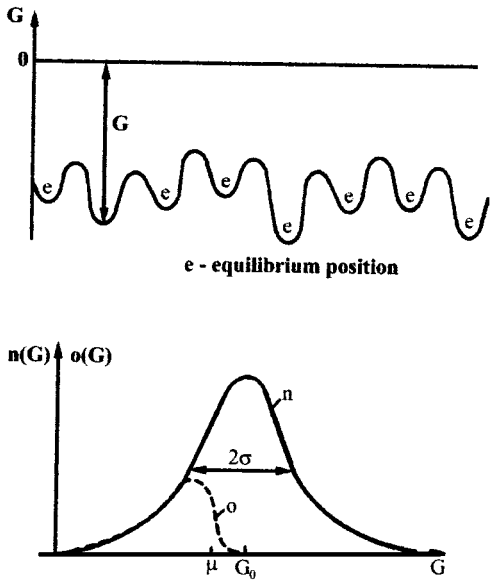

Figure 1. Potential trace for hydrogen in an amorphous metal, where dissolution from a reference state requires the free enthalpy G. The distribution $n(G)$ of the free enthalpy is shown below. The occupation $o(G)$ of the equilibrium sites e is governed by Fermi-Dirac statistics [21].

amorphous alloys lack long-range order (LRO), hydrogen atoms might occupy a wide variety of interstitial sites, resulting from a distribution of both chemical and geometrical configurations in the amorphous structure. Hence, a broad continuous distribution of interstitial site energies is used to explain the concentration dependence of the chemical potential of hydrogen and its diffusivity in amorphous metals. Due to theoretical considerations [30], the shape of this energy distribution can be related to the shape of the first peak of the radial distribution function (RDF), which is usually assumed to be of a Gaussian form for amorphous metals. Thus, assuming that sites for hydrogen atoms in amorphous alloys have different potential energies (see figure 1), the density of sites (n) is expressed [19–21] by the Gaussian function:

$$n(G) = \frac{dN}{dG} = \frac{1}{\sigma\sqrt{\pi}} \exp\left[-\left(\frac{G - G^o}{\sigma}\right)^2\right] \tag{1}$$

where dN is the number of sites available for hydrogen at energy G within the interval dG, G^o is the mean energy related to a standard state, and σ is the width of the Gaussian function. Applying Fermi-Dirac statistics, the occupancy is obtained:

$$o(G) = \frac{n(G)}{1 + \exp\left(\dfrac{G - \mu}{RT}\right)} \tag{2}$$

where μ is the chemical potential of hydrogen. The concentration of hydrogen atoms is then obtained by integration of Eq. (2):

$$c = \int_{-\infty}^{\infty} o(G)\, dG \tag{3}$$

where the Fermi-Dirac distribution may be approximated by a step function, yielding:

$$2c = 1 \pm \mathrm{erf}\frac{G^o - \mu}{\sigma} \quad + \text{for } G^o < \mu \quad \text{and} \quad -\text{for } G^o > \mu \tag{4}$$

Harris and co-workers [23, 24] suggest a model for the general shape of the site-energy distribution and hydrogen absorption capacities of binary ETM-LTM amorphous alloys. This model is based on accurate measurements of the hydrogen chemical potential in amorphous Zr-Ni alloys by the electrochemical method. An assumption is made that the structure of these amorphous alloys is composed of packed, distorted tetrahedra, formed by a random distribution of the two kinds of atoms. Calculations are made of the probability of finding a particular type of tetrahedra and of the energy of a hydrogen atom in a tetrahedron. A bell-shaped function is chosen to describe the distribution of site energies about these mean values, due to the range of distortions about ideal tetrahedral structures. The maximum hydrogen content in amorphous Zr-Ni alloys, as predicted by this model, agrees excellently with the experimental data. Harris and Curtin thus proceed to apply this model to other systems, including Zr-Ni alloys prepared by mechanical alloying [25] and ternary Zr-Ni-B and Zr-Nb-Ni amorphous alloys [26]. A comprehensive review of their works is given in reference [27].

Results of neutron diffraction and scattering experiments [15, 31, 32], however, suggest the occupancy of other types of sites than that, on which the model of Harris et al. is critically based. This apparent contradiction may result from the fact that while the electrochemical measurement probes the site occupancy in a particular range of chemical potentials, neutron diffraction and scattering experiments give information on the average configuration of all occupied sites [33].

Rush et al. [34] were the first ones to use hydrogen vibrations as a probe for investigating the local topology in the amorphous structure. In their work, they compare the vibrational spectra of glassy and crystalline TiCuH (figure 2). Large differences between the density of states distributions for the two samples are evident. In the amorphous alloy, the peak occurs at the same frequency as in the crystalline alloy, but with a strongly increased width. Thus, the hydrogen sites occupied in the amorphous and crystalline structures may be regarded, on the average, to be very similar (short-range order). The large width indicates that the tetrahedron may be heavily distorted and fluctuates in its chemical composition. The wing towards frequencies below 100 meV may also show that octahedral site occupation occurs as well. The observation of the broader density of states disagrees with the microcrystalline or microcluster model for amorphous metals, in which the local environment would not differ from that of the crystal [35]. Later experiments on other glasses (e.g., ZrNiH [36–38] and Zr_2Pd [39]) qualitatively all revealed the same result—the local hydrogen spectra in the amorphous substance center around similar frequencies to those in the crystalline state, but the frequency distributions are generally much broader and washed out. Thus, on the basis

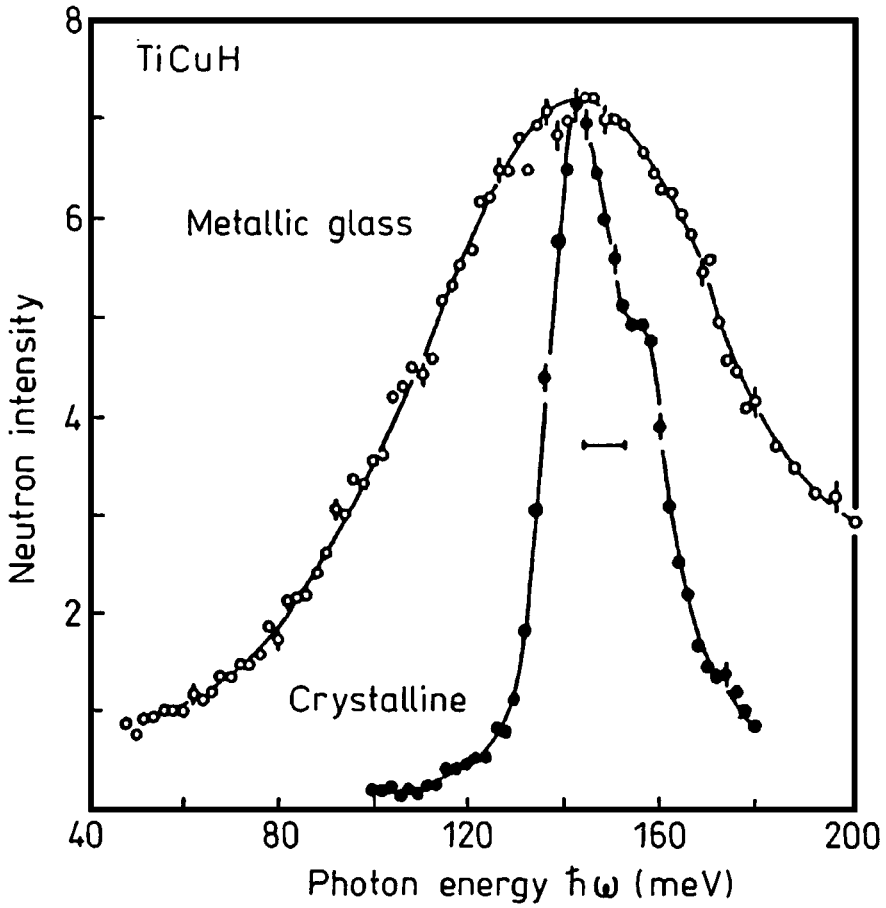

Figure 2. Neutron spectra measured at 78 K for crystalline $TiCuH_{0.93}$ and amorphous $TiCuH_{1.3}$. The energy resolution (FWHM) near the peak is indicated by the horizontal bar [34].

of these measurements, we may conclude that the hydrogen atoms remain in amorphous metals essentially at the same polyhedral sites as in the crystalline counterparts; changes in topology are therefore rather restricted [35].

The idea that hydrogen might occupy in amorphous alloys interstitial sites, which are similar to the octahedral and tetrahedral interstitial sites in crystalline alloys, is suggested on the basis of other experiments as well (see, for example, [20, 40]). This idea is based in these works on measurements of similar values of hydrogen solubility [40], frequency factor (D_0) and activation energy for diffusion (Q) [20] in amorphous and in fcc structures.

3. Absorption-desorption characteristics

Amorphous alloys are thermodynamically metastable, and decompose into multiple crystalline phases when heated to the crystallization temperature, $T_{\text{cryst}} \sim 300$–$500^{\circ}$C, depending

on the chemical composition of the alloy. Thus, in charging amorphous alloys with hydrogen, either electrochemically or from the gaseous phase, care must be taken not to raise the temperature above T_{cryst}. We cannot activate the surface by heating in vacuum or in H_2 gas, as is usually done in the case of crystalline samples, but generally circumscribe ourselves to abrading the surface with emery paper and cleaning ultrasonically in acetone and ether. Coating with a Pd overlayer after cleaning by argon-ion sputtering has also been known to be effective [33].

In crystalline alloys, if a phase transformation occurs in the metal-hydrogen system, the chemical potential of hydrogen (or its pressure) remains constant within the two-phase region, although the total hydrogen concentration increases. However, one of the most characteristic changes in going from crystalline to amorphous alloys is the disappearance of the plateau in the pressure-concentration isotherms [12, 15, 22, 33], as evident from figure 3 for a $Zr_{50}Ni_{50}$ alloy [41]. Spit et al. [42, 43] as well report the absence of plateau in the *p-c-T* curves of Ni(Zr, Ti) amorphous alloys. They relate it either to a rather low critical

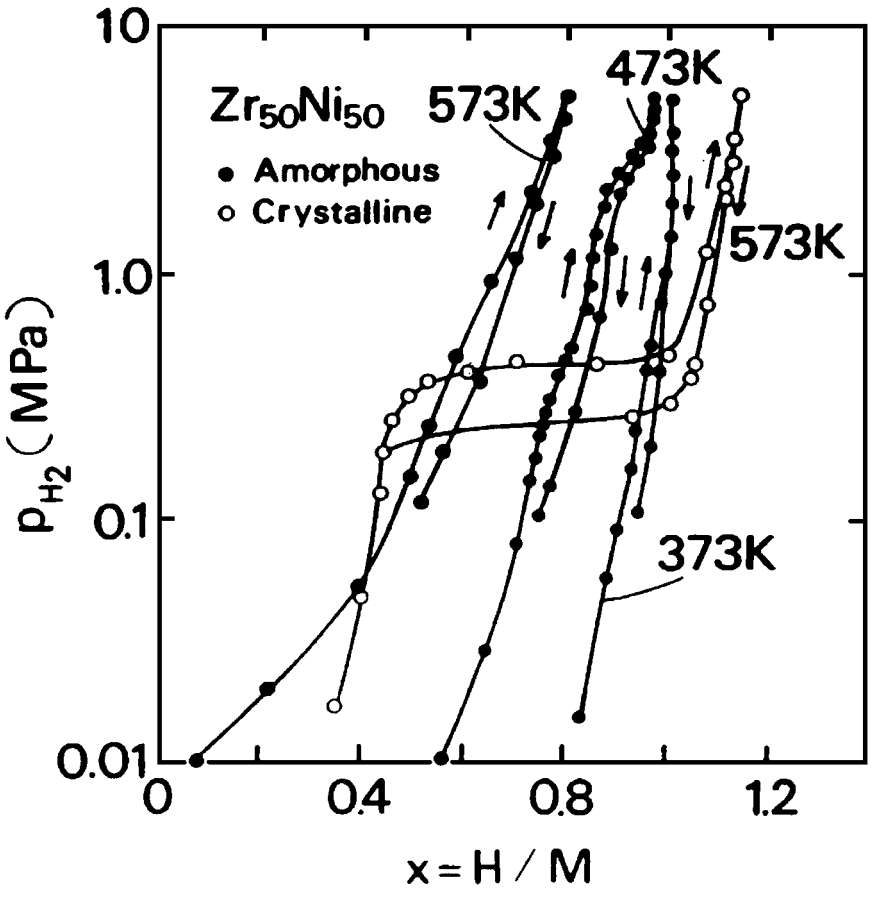

Figure 3. Pressure-composition isotherms for hydrogen in amorphous and crystalline $Zr_{50}Ni_{50}$ [41].

temperature of the amorphous hydride or to an absence of phase separation, even at low temperatures. The first explanation, however, is difficult to prove because of prohibitively long equilibrium times. Referring to the second explanation, since plastic deformation that accompanies hydride formation may be avoided, and consequently destruction during cycling is not expected to occur, Spit et al. suggested to use amorphous metals for hydrogen storage applications.

Hysteresis effects, as evident in figure 3, have also been observed in other cases. However, they cannot be said to be a general property because they were not observed, for example, in a Ti-Fe film sputter-deposited on Al-foil. The existence of hysteresis is quite unusual if there is no two-phase separation involved. It may be due, at least in part, to changes in the kinetics of absorption/desorption of hydrogen caused by changes in the surface compositions, but may also be due to some structural relaxation. The origin of the observed hysteresis effects thus is not fully understood yet [33].

It may be appropriate here to mention some aspects of the volume changes caused by hydrogenation of metallic glasses. Hydrogenation of amorphous metals and alloys causes volume expansion in most cases [14, 44, 45], with the volume increase per hydrogen atom being very similar to that observed in crystalline metals ($\sim 2.9 \cdot 10^{-3}$ nm^3 [46]). However, a possible effect of elastic interactions between hydrogen atoms, namely a linear decrease of the heat of solution with increasing hydrogen concentration, has not been observed. Admittedly, it is very difficult to isolate this term in the presence of site-energy distribution [33]. One other observation about the volume changes is that in $Pd_{80}Si_{20}$ and $Ni_{34}Pd_{48}P_{18}$, a normal volume expansion of about $2.5 \cdot 10^{-3}$ nm^3 occurs at hydrogen concentrations larger than about 10^{-4}, whereas at lower concentrations a negative volume change of about $-1.5 \cdot 10^{-3}$ nm^3 takes place. Stolz et al. suggest [47] a qualitative explanation to this change of the partial molar volume of hydrogen from negative values at low hydrogen concentrations to increasing positive values with increasing hydrogen content. According to this attitude, since the potential between host atoms and hydrogen atoms changes from negative (attractive) to positive (repulsive) values with decreasing distance of the atoms, at low concentrations hydrogen occupies large interstices and attracts neighboring host atoms, whereas at higher concentrations hydrogen atoms have to be squeezed into the remaining smaller interstices.

Thermal desorption spectroscopy (TDS) has been used in several studies to characterize the kinetics of hydrogen desorption from amorphous alloys and its interaction with structural defects. The results of these studies support some models of site energies distribution for hydrogen in amorphous metals, as previously discussed in our paper. Lee and Lee [48] investigated the desorption from both as-received and relaxed amorphous $Pd_{80}Si_{20}$. Figure 4 illustrates the general characteristics of desorption from an as-received alloy containing different concentrations of hydrogen. It can be noticed that as the hydrogen concentration increases, the desorption peak increases in height and shifts toward lower temperatures, in accordance with Kirchheim's model [19–22]. As the evolution rate curves merge at the high temperature side, it was concluded that hydrogen fills the low-energy sites (i.e., high activation energy for desorption) first. Finding that hydrogen solubility was decreased by structural relaxation, it was suggested that excess free volume quenched into the glass was eliminated and redistributed during the relaxation, thus decreasing the width of the site energy distribution.

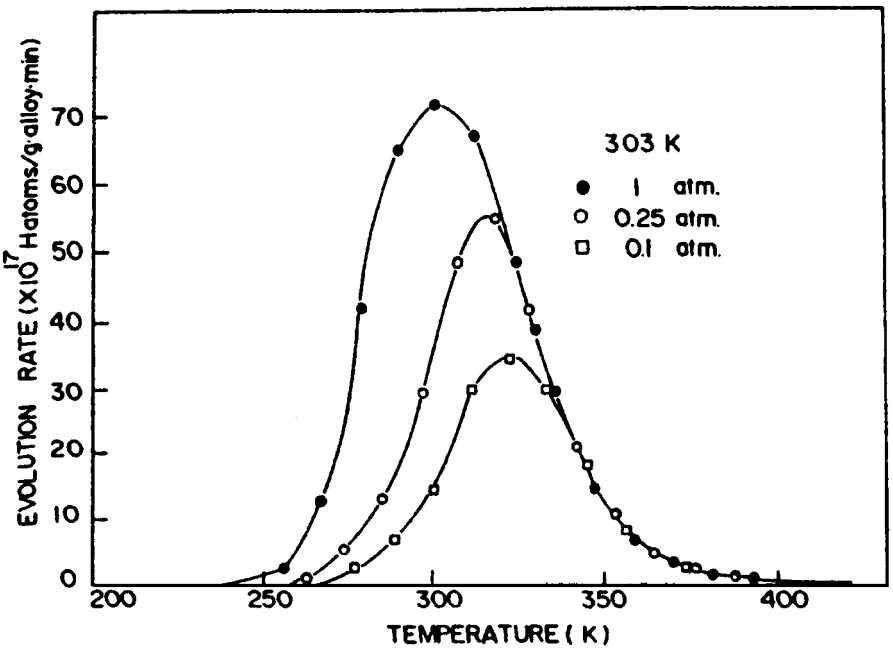

Figure 4. Concentration dependence of hydrogen evolution rate peak in amorphous $Pd_{80}Si_{20}$ after hydrogen gaseous charging at 303 K [48].

Eliaz et al. [49] concluded on the basis of TDS results that amorphous $Fe_{80}B_{11}Si_9$ can accommodate hydrogen with a wide distribution of site energies. The combination of TDS and electron microscopy was used to characterize the type of traps for hydrogen in this alloy. A low hydrogen solubility, varying between $1.3 \cdot 10^{-5}$ and $2.4 \cdot 10^{-5}$ H/M, and a detrapping activation energy of 33.5 ± 14.1 kJ/mol (0.35 ± 0.15 eV/atom) were calculated for the charging parameters applied in this research.

4. Hydrogen solubility

Hydrogen solubility is defined as the hydrogen concentration at a given hydrogen pressure (or chemical potential, or e.m.f.). For crystalline metals at sufficiently low pressures ($p < 1$ MPa), the solubility is usually described by Sieverts' law:

$$c = K\sqrt{p} = K_0 \exp(-E_k/RT)\sqrt{p} \tag{5}$$

where c is the atomic hydrogen concentration in the solid, K is the hydrogen solubility in the metal, p is the partial pressure of H_2 in the gaseous phase, K_0 is the solubility constant, E_k is the activation energy of solution, R is the constant of ideal gases and T is the absolute temperature.

The Sieverts' law plots [41, 44] for amorphous Zr-Ni alloys are shown in figure 5. The positive strong deviation from Sieverts' law at high hydrogen concentrations has also

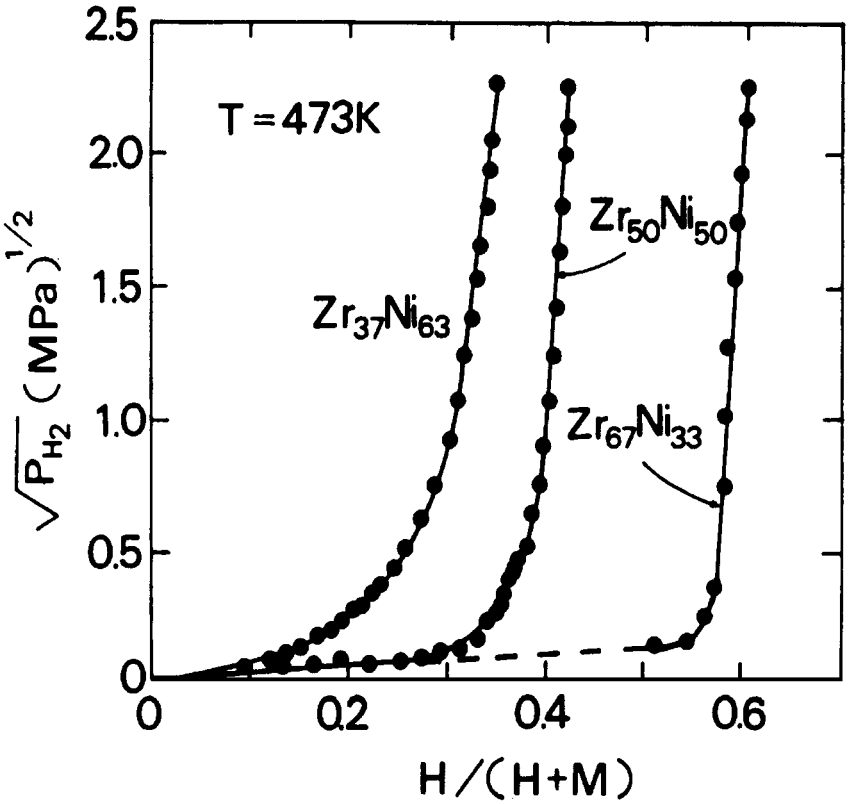

Figure 5. Sieverts' law plots of the pressure-composition isotherms in amorphous Zr-Ni alloys [41, 44].

been observed in other cases and is believed to be a general feature of amorphous alloys. This deviation can be related to the successful entry of hydrogen atoms into higher-energy states [33].

Figure 5 shows that the maximum hydrogen content absorbed in the amorphous Zr-Ni alloy is about two-thirds of that in crystalline Zr-Ni under the same conditions of temperature and pressure. The case of the Zr-Ni alloy is considered to be rather unusual. Amorphous alloys often have larger hydrogen absorption capacities than the corresponding crystalline alloys [12, 14, 15, 50]. This may be due to much less restricted sites for hydrogen in the amorphous structure. It should be mentioned, however, that some contradictory results could be found in the literature. Bowman [16], for instance, reports that many metallic glasses tend to absorb less hydrogen than their crystalline counterparts. He explains this behavior by the inherent structural disorder in the amorphous phase, which might restrict the number of interstitial sites that are favorable for hydrogen occupancy.

Metallic glasses suitable for hydrogen storage applications are based on a hydride-forming element. Typical examples are ETM-LTM metallic glasses (combinations of Y, Ti, Zr and Hf with Fe, Ni, Cu, Rh and Pd), or RE-LTM metallic glasses (combinations of

Table 1. Hydrogen solubilities in various materials at 0.1 MPa H_2.

Material	Structure	Solubility H/M	Technique[a]	Ref.
α-Fe	bcc	$1.6 \cdot 10^{-8}$	GP (at 19°C)	[53]
310 stainless steel	fcc	$1.0 \cdot 10^{-4}$	GP (at 19°C)	[54]
Ni	fcc	$1.3 \cdot 10^{-5}$	TD (at 30°C)	[55]
$Fe_{40}Ni_{40}P_{14}B_6$	amorphous	$5.0 \cdot 10^{-5}$	GP (at 40°C)	[52]
$Fe_{40}Ni_{38}Mo_4B_{18}$	amorphous	$4.3 \cdot 10^{-5}$	EP (at 30°C)	[40]
$Ni_{64}Zr_{36}$	amorphous	$3.5 \cdot 10^{-1}$	EP (at 60°C)	[20]
$Pd_{77.5}Cu_6Si_{16.5}$	amorphous	$2.5 \cdot 10^{-2}$	EP (at 22°C)	[20]
$Ni_{49.9}Pd_{31.8}P_{18.3}$	amorphous	$7.0 \cdot 10^{-4}$	EP (at 72°C)	[20]

[a]GP: gas permeation; EP: electrochemical permeation; TD: thermal desorption.

La, Ce, Pr, Sm and Gd with Co and Ni) [51]. Whereas the solubility of hydrogen in these alloys is quite high, the solubility of hydrogen in amorphous alloys containing no hydride former is far lower. At 0.1 MPa and 60°C, for example, $Ni_{64}Zr_{36}$ absorbs hydrogen up to a content of 0.4 H/M [43] from the gaseous phase, while at 0.1 MPa and 40°C $Fe_{40}Ni_{40}P_{14}B_6$ dissolves only about $5 \cdot 10^{-5}$ H/M [52].

Table 1 summarizes the solubilities of hydrogen in several amorphous and crystalline alloys. Since the solubility of these materials is quite small at room temperature, some of these values are estimated from the high temperature data. The similarity between the solubility values in fcc and in amorphous structures (at least at low concentrations) is clear and may suggest that in both cases hydrogen occupies similar sites.

5. Hydrogen diffusivity

In this part, we review some of the experimental studies that have been carried out to evaluate the diffusion behavior of hydrogen in glassy metals, as well as theoretical concepts and computer modeling. A special emphasis is made on the observed deviations from the Arrhenius behavior. For more information on this topic, we recommend on the comprehensive reviews of Bowman [16] and Richter et al. [35].

Experimental measurements of hydrogen diffusivity in amorphous metals have been carried out by many researchers. Lin and Perng [56] studied hydrogen permeation in amorphous $Fe_{40}Ni_{38}Mo_4B_{18}$ alloy using the electrochemical permeation (EP) technique in the temperature range of 30–75°C. Hydrogen diffusivity was found to increase with charging current density. This increase in diffusivity as hydrogen concentration increases was rationalized on the basis of the structural features of amorphous alloys. It was also suggested that the diffusivity was affected only by "intrinsic" concentration and trapping effects, without any existance of surface impedance. In another work [57], Lin and Perng obtained the concentration and diffusivity of hydrogen in the same alloy by means of both electrochemical charging and thermal evolution experiments. Hydrogen diffusivity in this alloy at room temperature was on the order of 10^{-10} cm^2/s.

Latanision et al. [58] studied hydrogen absorption in metalloid-containing glasses using the EP technique. The materials examined were $Fe_{32}Ni_{36}Cr_{14}P_{12}B_6$, $Ni_{81}P_{19}$ and $Fe_{40}Ni_{40}P_{14}B_6$. The diffusivities of hydrogen determined from either rise or decay transients were of the order of $6 \cdot 10^{-11}$ and $8 \cdot 10^{-11}$ cm^2/s in $Fe_{40}Ni_{40}P_{14}B_6$ and $Fe_{32}Ni_{36}Cr_{14}P_{12}B_6$, respectively. It was observed that if the cathodic charging current exceeded a certain limit, the permeation flux began to decrease with time rather than achieving a steady state. This observation was associated with trapping of hydrogen in voids introduced during fabrication. The authors believe that when the pressure in the voids achieved a sufficient magnitude, the voids would have expanded, and in growing acted as larger sinks for hydrogen.

Hara and Latanision [59] examined the diffusivity of hydrogen in amorphous $Ni_{77.5}Si_{7.9}B_{14.6}$, in comparison with those in the corresponding crystalline alloys, by means of the EP technique. The amorphous alloy was crystallized at 330 and 400°C, which were below and above the critical temperature of crystallization, respectively. The diffusivity was observed to change as a result of the aging treatments. This change in the diffusivity was dependent on the nature of the microstructure produced by aging.

Flis et al. [60] measured the permeation of hydrogen through various iron-based and nickel-based amorphous alloys by electrochemical methods. The results of these measurements were then used to explain the susceptibility of the different alloys to hydrogen embrittlement. It was concluded that the observed differences in hydrogen embrittlement could not be related to differences in diffusivities or solubilities of hydrogen in the alloys. Instead, the degree of hydrogen embrittlement was found to be dependent strongly on the ease of hydrogen entry into the alloys.

Kirchheim et al. [20] used the EP technique to measure the solubility and diffusivity of hydrogen in amorphous $Pd_{77.5}Cu_6Si_{16.5}$ and $Ni_{49.9}Pd_{31.8}P_{18.3}$. The diffusivity was found to be rather high ($\sim 10^{-8}$ cm^2/s) and was dependent on temperature and also on the concentration of soluted hydrogen, even at very low hydrogen levels, in contrary to crystalline metals. This study was the first to describe the diffusivity dependence on concentration and temperature by a model, considering the amorphous metal to be composed of a spectrum of defects.

Table 2 summarizes the values of frequency factor and activation energy for diffusion of hydrogen in several amorphous alloys. For comparison, the equivalent values for hydrogen

Table 2. Frequency factors (D_0) and activation energies (Q) for diffusion of hydrogen in amorphous alloys. When measured, hydrogen concentration in the bulk is also presented.

Material	Concentration C_0 (H/M)	Frequency factor D_0 (cm^2/s)	Activation energy Q (eV/atom)	Ref.
$Pd_{80}Si_{20}$	—	$3.0 \cdot 10^{-3}$	0.25	[61]
$Pd_{77.5}Cu_6Si_{16.5}$	$2.05 \cdot 10^{-3}$	$1.0 \cdot 10^{-2}$	0.34	[20]
$Pd_{77.5}Cu_6Si_{16.5}$	$3.2 \cdot 10^{-5}$	1.4	0.50	[20]
$Fe_{40}Ni_{38}Mo_4B_{18}$	$4.8 \cdot 10^{-2}$	$1.56 \cdot 10^{-4}$	0.36	[56]
$Fe_{40}Ni_{38}Mo_4B_{18}$	$8.0 \cdot 10^{-3}$	$2.27 \cdot 10^{-4}$	0.38	[56]
$Ni_{77.5}Si_{7.9}B_{14.6}$	—	$7.08 \cdot 10^{-4}$	0.46	[59]
Pure crystalline Ni	—	$7.05 \cdot 10^{-3}$	0.42	[62]

diffusion in pure crystalline nickel are given too. Again, a similarity between the values for amorphous and fcc structures is evident.

Although the exact mechanisms of hydrogen diffusion in amorphous metals remain controversial, several characteristics seem to be on reasonably firm ground. First, the kinetics of hydrogen diffusion is many orders-of-magnitude faster than the diffusion kinetics for heavier interstitials [63, 64] or the metal atoms [63, 65] in metallic glasses. This is not surprising when one considers the smaller effective radius of a hydrogen atom as well as its light mass. However, evidence is reported [16] for an enhancement in the metal atom mobility in amorphous $Zr_{60}Ni_{40}H_x$. This behavior is attributed to the weakening of the metal-metal bonds due to lattice expansion during absorption of large amounts of hydrogen. Second, converse to the usual diffusion behavior in crystalline hydrides [33, 66], where mobility decreases with increasing hydrogen concentrations, the hydrogen jump rates in glassy hydrides often very rapidly become faster [19, 20, 67–73] as the hydrogen content is increased. Various studies [70, 72, 74–76] compared between the hydrogen diffusion properties of crystalline and amorphous alloys; greater mobility and smaller average values of activation energy were found for the glassy samples as long as $H/M > 0.01$.

Numerous theoretical concepts have been used to evaluate the diffusion of hydrogen in amorphous metals. Kirchheim [19] assumes a Gaussian distribution of equilibrium site energies to explain the concentration dependence of the chemical potential of hydrogen and its diffusivity in amorphous metals. According to this model, the effective diffusivity at low concentrations ($c \ll 1$) of hydrogen is given by:

$$D_{\text{ef}} = \frac{D^o \sigma \sqrt{\pi}}{RT} \exp\{\text{erf}^{-1}|2c-1|\}^2 \exp\left(\frac{G^o - \sigma \text{erf}^{-1}|2c-1|}{RT}\right) \tag{6}$$

where D^o is the diffusivity in a theoretical solid containing only sites of energy G^o, and σ is the width of the Gaussian distribution.

The diffusion coefficient for an interstitial atom in a disordered material was calculated by Kirchheim and Stolz [77] as a function of temperature and concentration for a distribution of site energies, but constant saddle energies, yielding:

$$D = D^o \frac{\partial}{\partial c}\left\{(1-c)^2 \exp\left(\frac{\mu}{RT}\right)\right\} \tag{7}$$

with a diffusion coefficient D^o given by:

$$D^o = D_0^o \exp\left(\frac{Q^o}{RT}\right) \tag{8}$$

where D_0^o is a prefactor, and Q^o is the average activation energy given by the difference between the constant saddle-point energy and the average value of the site energy distribution.

Two different approaches relate the diffusion rate to interstitial sites in the amorphous structure. According to Kijek et al. [28], as a result of a distribution in the size of interstitial sites in amorphous materials, the diffusion of interstitials is not random. According to this

approach, the diffusivity of a given atom in an amorphous material is expected to be smaller than in a fcc crystal, since the diffusion atoms may be trapped in bigger interstitial sites. On the other hand, Ahmadzadeh and Cantor [29] suggest that if the diffusion of interstitials is controlled by the rate of escape from octahedral sites, the effective activation energy for diffusion should be similar in amorphous and in fcc structures.

Several computer modeling, mainly based on Monte-Carlo (MC) simulations, have been used to forecast the diffusion of hydrogen in amorphous metals. Ahmadzadeh and Cantor [78] were probably the first ones to use the concept of varying site and saddle-point energies for light interstitial atoms diffusion and to run MC calculations for amorphous metals. Kirchheim and Stolz [67] used similar simulations to study the effect of presence/absence of distributions of site and saddle-point energies on the characteristics of hydrogen diffusion in amorphous metals. For a distribution of saddle-point energies it was shown that Eq. (7) still holds when using a value of Q^o which is slightly less than the difference between the mean values of the two energy distributions, indicating that the interstitial prefers to jump over the lower activation barriers. Other conclusions of this study [67] refer to deviations from the Arrhenius behavior, as discussed in detail in the following paragraphs.

NMR measurements have been used [16, 75, 76] to study hydrogen diffusion in metallic glasses. Comparing the temperature dependence of the τ_c^{-1} parameters in amorphous $TiCuH_{1.41}$ with the results for the crystalline hydrides $TiCuH_{0.94}$ and $TiH_{1.90}$ (figure 6), an enhanced hydrogen mobility with reduced activation energies is clearly evident, as is the distinct non-Arrhenius character for the amorphous hydride [35]. Very similar behavior has also been observed [76] for crystalline and amorphous Zr_2PdH_x. Although the protons preferentially occupy tetrahedral sites in both $TiCuH_x$ and Zr_2PdH_x, variations in hydrogen site occupancies or structure-sensitive changes in the allowed diffusion jump paths (e.g., the presence of octahedral intermediate sites) are assumed to be responsible for this behavior. The smaller U values derived from the lower temperature $T_{1\rho}$ data may be due to protons in less stable sites, or represent specific variations in the diffusion saddle-point configurations for the presumably dominant tetrahedral sites. As more information on the distributions of occupied proton sites is obtained for these amorphous hydrides, it should be possible to determine which cause is responsible [35].

When hydrogen diffusion parameters for intermetallic or amorphous alloys are determined over limited (100 degrees maximum) temperature ranges, the data is usually well represented [16, 68, 79] by the Arrhenius relation with specific activation energy. However, techniques that can monitor motion over wider temperature ranges (e.g., NMR) often exhibit very anomalous temperature dependencies [16, 80], which simple Arrhenius models cannot describe.

Various concepts have been suggested to account for such deviations. One view is that the microscopic diffusion processes can consist of two basic kinds of jump: (1) relatively rapid motion, usually with smaller energies, within localized regions of the lattice that may involve only a portion of the hydrogen atoms and a subset of the allowed interstitial sites; and (2) jumps that permit movement of hydrogen between these regions, which will determine the long distance diffusion properties. Examples of this descriptive scheme are presented in [16, 81].

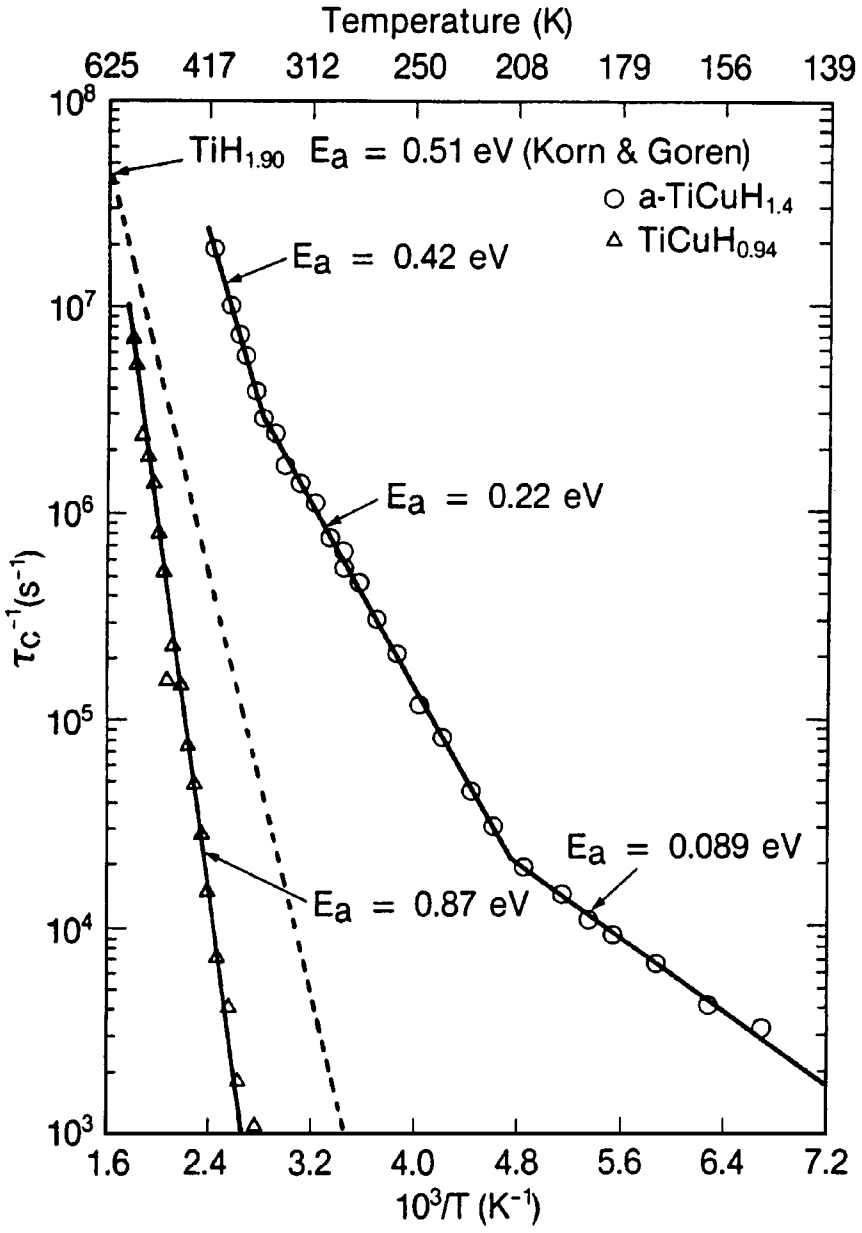

Figure 6. Comparison of the proton jump rates τ_c^{-1} for crystalline and amorphous $TiCuH_x$ derived from the T_1 relaxation times. Also shown are the results for crystalline $TiH_{1.90}$ [35].

A second possible view is to assume that various types of lattice disorder can lead to distributions of activation energies about the mean value Q, which would represent distinct jumps among equivalent sites in a defect-free host lattice. Kirchheim and Stolz [67, 82] have applied variations of a Gaussian distribution model for the Q values to explain hydrogen diffusion characteristics in amorphous alloys. Assuming [67] no distribution of site energies, either with or without distribution of saddle-point energies, the linear behavior of the Arrhenius plots for the diffusion coefficient was obtained. Allowing for a distribution of site energies, however, resulted in a pronounced negative curvature that was related to trapping. It should be noted, however, that many inconsistencies arise from the Gaussian distribution models. Markert et al. [83] required an asymmetric distribution function to improve fits of their proton T_1 and $T_{1\rho}$ relaxation times from amorphous $Zr_3RhH_{3.5}$, but even with this version they could not remove all disparities. Furthermore, Bowman et al. [16, 84] have described other inconsistencies that arise when distribution models are used to represent more extensive sets of NMR relaxation times from crystalline and glassy hydrides. PAC results [85–87] for amorphous Zr_2NiH_x do not reveal the presence of a broad distribution of activation energies. The strongest evidence, however, for the inadequacy of Gaussian distribution models comes from neutron scattering measurements [81, 88] and Monte Carlo simulations [89] on hydrogen diffusion in amorphous $Pd_{1-y}Si_yH_x$ alloys. The QNS results dictate a bimodal distribution of widely separated hydrogen-site energies that correspond to very different regimes for the jump rates. This behavior arises quite naturally from the simultaneous hydrogen-site occupancies in distorted Pd_6 octahedral and various tetrahedral sites as deduced from neutron vibrational spectra [88]. Consequently, prior applications [19, 20] of Gaussian distributions to represent the microscopic diffusion mechanisms in this system as well as other disordered hydrides must be treated with caution.

Recently, Eliaz et al. [90] showed that the deviation from Arrhenius law for the diffusion in amorphous metals may be linked to the temperature dependence of the short-range order. The latter enters the activation energy in a natural way by means of coordination numbers, which appear to vary with temperature. Figure 7 demonstrates the negative curvature in the diffusivity plot for hydrogen in amorphous iron, as predicted by this approach. We believe that this simple model may thus be used to study the tendencies in the diffusion behavior in amorphous metals under alloying, instead of using complicated and time-consuming Molecular-Dynamics or Monte-Carlo simulations.

6. Hydrogen effects on the thermal stability

Hydrogen effects on the thermal stability of metallic glasses were reported in various papers. Bowman [16] explains that the exothermic reactions between hydrogen and most metallic glasses that can absorb large quantities of the gas release additional energy, which may cause crystallization or decomposition. Cantrell and Bowman [91] conducted DSC measurements from several Zr-based metallic glasses and their amorphous hydrides. Whereas only exothermic transitions were observed in the DSC curves of the uncharged metallic glasses, both exothermic and endothermic peaks could be found for the amorphous hydrides. The authors primarily associate the endothermic transitions with evolution of hydrogen from the hydride [91–93]. In fact, the endothermic peak temperatures were found [91, 92, 94]

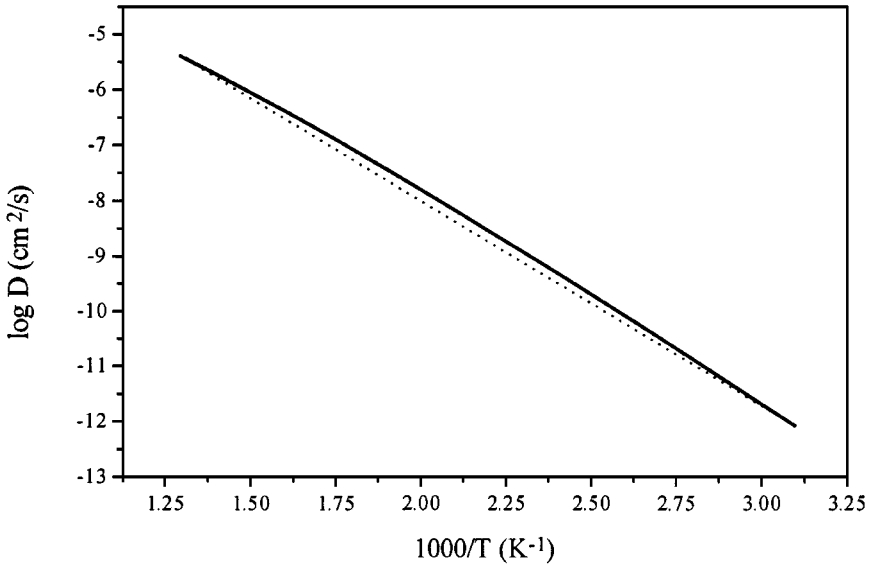

Figure 7. Arrhenius plot of the diffusivity of hydrogen in amorphous Fe. Solid line was calculated using the temperature-dependent activation energy. The dotted line allows to see the deviation from the linear dependence [90].

to decrease systematically as the hydrogen content increases. This behavior is consistent with the model of occupation of less stable interstitial sites by hydrogen as its concentration increases. Another characteristic of hydrogen effects on the thermal stability is that the exothermic transitions usually occur at lower temperatures for the amorphous hydrides than for the original metallic glasses [91, 92, 94–99]. Furthermore, the decrease in the DSC exothermic transition temperatures has been accompanied with substantially smaller activation energies of crystallization for amorphous $TiCuH_x$ [98] and Zr_3RhH_x [92]. Since diffusion plays a crucial role in the crystallization phenomenon, the decreased stabilities of most amorphous hydrides relative to the original glassy alloys implies greater mobilities for the metal atoms as well as hydrogen in the amorphous hydrides.

Hydrogenation of a crystalline or amorphous material may alter its atomic structure; e.g. it can change the lattice symmetry or cause chemical or topological short-range reordering as amorphization in crystalline sample or clusterization. Such changes can be followed by measuring the structure-sensitive magnetic properties, such as stress induced anisotropy, coercive force and demagnetizing factor [100].

Garaguly et al. [101] investigated the process of hydrogen absorption and desorption in $Ni_{67-x}Cu_xZr_{33}$ glassy alloys. They report that in some cases the original diffusive ring in SAD (which is characteristic of the amorphous state) splits into two new diffuse rings. This splitting is explained in terms of phase separation taking place in the amorphous matrix.

During the early eighties many studies were reported on the hydrogen storage capacity of amorphous Cu-Ti, Cu-Zr and Ni-Zr alloys, due to the ability of the second metal to form hydrides [12, 14]. These experiments revealed that Cu-Zr is recrystallized rapidly mostly

as a result of the chemical reaction between the alloy and hydrogen rather than the physical dissolution of hydrogen in the bulk.

Katona et al. studied [102, 103] the catalytic properties of Cu-Zr and Cu-Ti metallic glasses in the dehydrogenation of various alcohols. Under the conditions of activation or during the reaction, the catalyst ribbons were exposed to hydrogen, resulting in the crystallization of the alloys [102]. This particular process generated a stable and active catalyst with orders of magnitude higher surface area [102, 103]. SEM and SAM experiments showed that the surface was populated by Cu particles. It was proved that these particles were derived from the segregation of Cu from the bulk to the surface due to the effect of hydrogen [104]. In another work, Katona et al. [105] showed that hydrogen treatment of a rapidly quenched amorphous Cu-Zr ribbon results in substantial structural changes. Depending on the duration of hydrogen treatment, the temperature and the hydrogen pressure, complex transformations took place. A part of the absorbed hydrogen could react with the alloy components to bring about the complete decomposition of the original amorphous phase. As a result, mixed crystalline phases (Cu and Cu_xZr_y compounds) and ZrH_2 were formed with the concomitant segregation of Cu to the surface. No similar changes, however, could be induced by hydrogen treatment of amorphous Cu-Ti and crystalline Cu-Zr alloys.

Lazarova et al. [106] studied the effect of electrochemical hydrogen charging on the thermal stability and Curie temperatures of amorphous $Fe_{79}B_{14}Si_7$ and $Fe_{60}Co_{25}B_{15}$. It was concluded that hydrogen had no significant effect on the thermal stability of these alloys, nor on the two-stage character of their crystallization process. In addition, no significant effect of hydrogen on the kinetics of the isothermal crystallization was observed.

Spassov and Tzolova [107] investigated hydrogen solubility and its effects on the crystallization processes of Cu-Ti and Ni-Ti metallic glasses. In both cases, a dependence of the crystallization products on the hydrogen content was observed. In the Cu-Ti system, hydrogenation led to a significant decrease in thermal stability as a result of phase separation and to the formation of microcrystalline structure after crystallization. In the Ni-Ti system, on the other hand, hydrides of both Ni and Ti were formed, then decomposed during thermal treatment, and finally—the same crystalline phases as in the uncharged alloys were formed.

Recently, Zander et al. [108] investigated in detail the absorption kinetics and storage ability as well as the stability of hydrogenated amorphous and quasicrystalline $Zr_{69.5}Cu_{12}Ni_{11}Al_{7.5}$ alloys. The DSC plots exhibited a two-step reaction in glassy $Zr_{69.5}Cu_{12}Ni_{11}Al_{7.5}$: formation of icosahedral quasicrystals followed by decomposition of the quasicrystals into the stable crystalline phases. With increasing hydrogen content, the peak for quasicrystal formation was shifted to higher temperatures. Decomposition of the quasicrystals, however, was moved to lower temperatures with increasing hydrogen content. Figure 8 exhibits the X-ray diffraction pattern after annealing at 400°C of glassy ribbons as a function of prior charging to different hydrogen contents. Hydrogen contents of $H/M < 0.05$ were found to reduce the number of quasicrystals formed during annealing. In the XRD pattern, all peaks of the icosahedral phase became weaker, thus indicating a smaller amount of quasicrystals. TEM investigations confirmed that this was due to a smaller number of quasicrystals; growth, however, seemed to be unaffected. This observation may explain the observed shift of the first peak in the DSC (i.e., the formation of quasicrystals) to higher temperatures. At higher hydrogen contents, instead of the quasicrystalline phase,

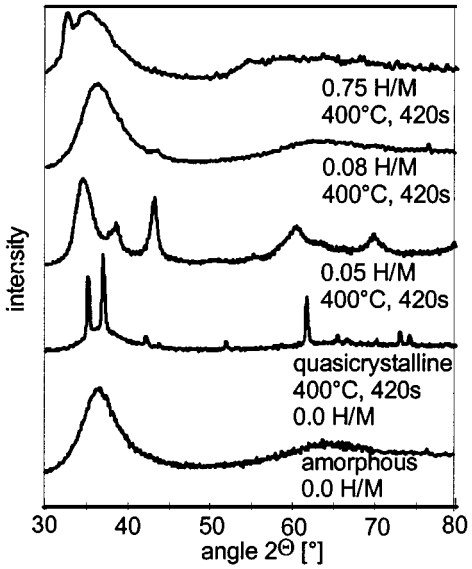

Figure 8. X-ray diffraction of uncharged as well as hydrogenated amorphous $Zr_{69.5}Cu_{12}Ni_{11}Al_{7.5}$ ribbons after annealing for 420 s at 400°C. For comparison, the XRD profile of the uncharged quasicrystalline alloy is presented too [108].

a tetragonal one with lattice parameters close to Zr_2Ni was formed. At hydrogen contents up to about $H/M = 0.6$, the amorphous state seemed to be stabilized as the number of nucleated crystals decreases significantly. This might result from phase separation into two amorphous phases, which leads first to elimination of quenched nucleation sites. Further charging to much higher H/M led probably to a progressive phase separation, followed by easy nanocrystallization of ZrH_2 and phases with reduced Zr-content. A similar destabilizing phase separation was reported by Menzel et al. [109] for binary Cu-Ti and Ni-Ti metallic glasses.

7. Hydrogen embrittlement of amorphous alloys

It has long been recognized that hydrogen may embrittle many crystalline metals and alloys. The embrittlement is manifested by the non-ductile fracture mode, reduced ductility and reduced tensile strength. Several mechanisms have been proposed to explain hydrogen embrittlement in crystalline materials. The most common ones are the high-pressure bubble formation [110], reduction in surface energy (adsorption mechanism) [111], reduction in the lattice cohesive force (decohesion mechanism) [112], hydrogen interaction with dislocations [113–117], and hydride formation [118, 119].

Nevertheless, it has also been found that some metallic glasses are susceptible to hydrogen embrittlement. Since amorphous alloys are distinguished from crystalline alloys in their deformation behavior (e.g., dislocations are absent, and fracture occurs immediately after the

elastic region), the embrittlement mechanisms in amorphous alloys might be different from those in the crystalline counterparts. The study of hydrogen embrittlement is of significant importance for many applications of metallic glasses. In addition, it may also be useful for understanding the deformation and fracture mechanisms of metallic glasses in more detail. Hence, in this part we summarize some of the experimental work that has been carried out in this area.

Lin and Perng [120] investigated the effects of hydrogen on the tensile properties and fracture processes of amorphous $Fe_{40}Ni_{38}Mo_4B_{18}$ at room temperature. Specimens were tested at various strain rates in air or under different cathodic charging current densities. It was found that the different test conditions led to a change in fracture stress, but did almost have no influence on the slopes of the stress-strain curves. The degree of hydrogen embrittlement increased as the charging current density increased or as the strain rate decreased. When trying to correlate the degree of embrittlement with the hydrogen concentration within the specimen it was found, for example, that an average concentration of about $1.3 \cdot 10^{-2}$ H/M caused a reduction of about 25% in tensile strength. Microscopically, the fracture path changed from 45° to 90° with respect to the tensile axis when tested in air or charged with hydrogen, respectively. For hydrogen-charged specimens, most regions of the fracture surface were similar to those for uncharged ones, except they exhibited some cellular pattern. Thus, the embrittlement was attributed to heterogeneous nucleation of localized plastic deformation. Finally, it was found that before cracking took place, the strength of the alloy could be completely restored by the degassing of hydrogen. In this case, the fractographic feature was also recovered to that of the uncharged specimens.

In order to examine the effects of hydrogen on the mechanical properties of this alloy under conditions of low fugacity and without any corrosion effects, Lin and Perng [121] examined the susceptibility for hydrogen embrittlement of amorphous $Fe_{40}Ni_{38}Mo_4B_{18}$ in 1 atm hydrogen gas. When reduced-section specimens were used for the tensile test, the effect of hydrogen on the tensile strength under various strain rates was negligible. When the test was performed under more severe conditions of double-edge-notched specimens, the notch tensile strength was significantly reduced at slower strain rates. Microscopically, almost no difference was found between the notched specimens tested in air and hydrogen, a result that was explained by the very limited plasticity of the uncharged material.

Namboodhiri et al. [122] studied hydrogen embrittlement of $Ni_{40}Fe_6Co_{20}Cr_{12}Mo_6B_{16}$, $Ni_{40}Fe_{40}B_{20}$ and $Ni_{39}Fe_{39}Mo_4Si_6B_{12}$ alloys. The fracture stress was reduced to 20–40% of its value in air as a result of cathodic charging. Microscopically, a large number of microvoids of various sizes were observed in hydrogen-embrittled specimens. These voids appeared adjacent to shear planes and may have been produced by hydrogen. It was suggested that they grew, coalesced and produced veins on the slant shear planes of chevron patterns. Based on the fractographic observations, the researchers related the fracture to the mechanism of ductile fracture in metallic glasses [123].

Ashok et al. [124] studied the susceptibility of amorphous alloys to liquid metal embrittlement (LME) and hydrogen embrittlement. Four alloys were chosen: $Fe_{81.5}B_{14.5}Si_4$, $Fe_{81.5}B_{13.5}Si_{2.5}C_{2.5}$, $Fe_{40}Ni_{40}P_{14}B_6$ and $Fe_{40}Ni_{38}B_{18}Mo_4$. Hydrogen was introduced into the specimens by cathodic charging, followed immediately by either tensile tests or bend

ductility tests. Embrittlement by hydrogen, as indicated from the mechanical tests, was more severe than embrittlement by liquid metals. Fractographic examination led the authors to suggest that both liquid metal embrittlement and hydrogen embrittlement were a consequence of enhanced shear at crack tips.

Kawashima et al. [125] performed bending and tensile tests of amorphous $Fe_{65}Cr_5Mo_{12}C_{18}$ and $Fe_{60}Cr_{10}Mo_{12}C_{18}$ alloys during cathodic polarization in sulfuric acid or immersion in hydrochloric acid. Comparing the fracture surfaces and crack propagation velocity in amorphous alloys that had been embrittled by hydrogen with those embrittled by heat treatments and with originally brittle alloys, it was concluded that the mechanisms of crack propagation were identical in all cases.

Schroeder and Köster [126] conducted bending tests after electrochemical charging of amorphous Fe-Ni-B, Pd-Zr, Ni-Zr and Ni-Zr-B alloys. Hydrogen embrittlement was observed in these alloys after an incubation time, which significantly decreased as a result of annealing at temperatures below the crystallization temperature. It was concluded that the amount of free volume in the structure was dependent on the content of boron, and that at certain amount of boron the susceptibility for hydrogen embrittlement was maximal. The embrittlement was explained, assuming that hydrogen reduced the cohesion between interatomic bonds and/or the quenched-in excess free volume of the metallic glass.

Latanision et al. [58] used the combination of electrochemical permeation measurements and microscopic examinations of several amorphous alloys ($Fe_{32}Ni_{36}Cr_{14}P_{12}B_6$, $Ni_{81}P_{19}$ and $Fe_{40}Ni_{40}P_{14}B_6$) to relate the disintegration of specimens in the absence of external loads to intercracking between voids, which acted as traps for hydrogen.

Recently, Eliaz et al. [49] reported $Fe_{80}B_{11}Si_9$ to be significantly embrittled by hydrogen. Using the powerful combination of TDS and electron microscopy, the embrittlement phenomenon was related to trapped hydrogen via the mechanism of high-pressure bubble formation. As in the work of Latanision et al. [58], it was suggested that internal voids in the amorphous structure act as traps for the atomic hydrogen, where it combines to form molecular hydrogen. This molecular hydrogen inside voids might ultimately (i.e., after reaching a critical pressure value) produce interpressure that can shatter the specimen. In order to evaluate the effects of both high-pressures (to which the material might be exposed during electrochemical hydrogen charging) and hydrogen absorption on the mechanical properties of amorphous $Fe_{80}B_{11}Si_9$, Eliaz et al. [127] measured the spall strength of both as-received and hydrogen-charged specimens. For this purpose, laser-induced shock waves measurements, under conditions of strain rates larger than 10^7 s^{-1}, were conducted using a unique ORVIS (Optically Recording Velocity Interferometer System) diagnostic system. We believe that such measurements may also enable to distinguish between embrittlement mechanisms that depend on time (e.g., those related to dislocations transport in crystalline alloys or cracks propagation between bubbles in amorphous alloys) and those mechanisms that are less time-dependent (e.g., decohesion). However, more work still has to be carried out in this direction.

To summarize, some of the mechanisms that have been suggested to explain hydrogen embrittlement of crystalline alloys are probably irrelevant to amorphous alloys. These include, for example, all mechanisms related to enhancement or inhibition of dislocations transport. On the other hand, some unique mechanisms, e.g., filling of free volume,

might be responsible for the embrittlement of amorphous alloys. These, however, may be accompanied by traditional mechanisms such as high-pressure bubble formation and decohesion.

8. Potential applications

The interaction of hydrogen with amorphous metals and alloys has been studied extensively, as mentioned above, during the last two decades. These studies were motivated by either scientific or technological interest.

From a scientific point of view, hydrogen in amorphous metals may be used as a probe to study the structure of the amorphous state [12, 19, 20, 35]. Hydrogen has a very large incoherent scattering cross section for neutrons, and its mass is very small in comparison with most metals. Thus, it is possible to study metal-hydrogen systems by inelastic neutron scattering techniques and measure the hydrogen vibration both in-phase (acoustic) and out-of-phase (optical) with the metal atoms. Such measurements provide a unique local probe for investigating the local topology in the glassy state, as demonstrated by figure 2 and the relevant text in part 2 of this paper (structural models for hydrogen occupancy). It is also possible to compare the characteristics of hydrogen diffusion and hydrogen solubility in amorphous materials with the same characteristics in the counterpart crystalline materials, thus learning about the structure of the amorphous state. Such researches may also improve the understanding of hydrogen diffusion through grain boundaries and its interaction with structural defects (trapping) in crystalline metals [58].

As aforementioned, various structural models have been suggested in order to explain hydrogen occupancy, solubility and diffusivity in metallic glasses; most of them assume the existence of continuous distributions of site energies in the amorphous structure. Some of these models are supported by experimental results. Certain phenomena distinguish amorphous alloys from crystalline alloys in regard to hydrogen behavior; these include the disappearance of the plateau from the pressure-concentration isotherm, positive deviations from Sieverts' law at high hydrogen concentrations, non-Arrhenius behavior of hydrogen diffusion, more pronounced effects of hydrogen on thermal stability in amorphous metals, etc. We believe that much research still has to be carried out before we can suggest universal explanations for some of these interesting physical phenomena of hydrogen in amorphous metals.

From a technological point of view, various potential applications of amorphous metals are concerned with the exposure to hydrogen (e.g., alloying with hydrogen of components for the micro-electronic industry in order to improve the electrical properties, materials for hydrogen storage, devices for fusion reactors, etc.) [4]. Therefore, the study of hydrogen embrittlement, hydrogen diffusion, characteristics of hydrogen absorption and desorption (all reviewed in the present work), and hydrogen effects on the electrical and magnetic properties is of great importance.

Actual and potential applications of metal hydrides include hydrogen storage, batteries, fuel cells, purification or separation of hydrogen, isotope separation, hydrogen getters, heat storage, heat pumps and refrigerators, thermochemical hydride compressors, sensors and detectors, and catalysts [128, 129]. In recent years, interest in hydrogen technology has been revived by the desire to reduce environmental pollution due to automobile emissions, as well

as by the concern over our dwindling natural gas and petroleum reserves [51, 130, 131]. In such hydrogen technology, the storage of hydrogen is of utmost importance. The reversible storage of hydrogen in the form of metal hydride has several advantages over conventional gaseous and liquid H_2 storage. Hydrides offer pronounced volumetric advantages over compressed gas. In fact, hydrogen densities achievable with hydride containers approach those of liquid storage, a result of the fact that the hydrogen packing density within a given hydride crystal is usually significantly higher than that of liquid hydrogen. Hydrides also give excellent insurance that the hydrogen released is of very high purity. Reactive species, such as O_2, H_2O and CO, tend to be gettered by the hydride, and inert species, such as N_2 and CH_4, can be purged away during the first few percent of discharge. Thus, hydride storage units are often used in special applications where extremely high-purity H_2 is required (e.g., as gas chromatograph carrier gas or for high-purity furnace atmospheres) [128]. In addition, because of the low pressures and near-ambient temperature involved in the use of metal hydrides, they are generally viewed to be a safer means of handling and storing hydrogen than cryogenic liquid and compressed gas. Hydrogen gas containers are extremely heavy and bulky, and hydrogen, which is nature's best example of an ideal gas, is very difficult to compress, inasmuch as low-viscosity hydrogen gas leaks past conventional compressor seals. Although cryogenic liquid hydrogen storage might be ideal for the aerospace industry, its applicability for everyday transportation seemed for years to be very limited. First of all, liquefied hydrogen costs much more than gaseous hydrogen, since hydrogen liquefaction takes place only at temperatures below 33 K. Furthermore, expensive highly-insulated containers are required for liquid hydrogen to minimize boil-off losses. Other major factors hindering the utilization of cryogenics in ground vehicular transportation are the high consumption of primary energy and the phenomena of flash-off and boil-off. The main drawbacks of hydride storage, however, are relatively low hydrogen weight percentages, high cost of the intermetallic compounds, and need to invest in heat exchangers for the storage containers.

One of the most active and interesting uses for metal hydrides has been as a carrier of hydrogen fuel for motor vehicles. Hydrogen recovery is obtained in this case by simply heating the material by the exhaust gas. Although the research for passenger vehicles powered by metal hydrides continues, there is a growing tendency toward liquid hydrogen vehicles. It could be claimed [128] that the lower weight associated with liquid hydrogen production (in comparison to hydride storage) offsets the higher cost of liquid hydrogen production (in comparison to gaseous hydrogen), so that for vehicle ranges greater than 200 km liquid hydrogen is preferred over hydrides. Below 200 km, however, especially when safety is considered, hydrides seem to have the economic edge.

Increasing R&D budgets have also been invested during the last few years in an effort to develop vehicles driven by fuel cells. Several of the major automobile manufacturers, including Volvo, Volkswagen, Nissan and Chrysler, have all begun experimenting with hydrogen-powered vehicles. Much information on these experiments is available in the internet (see, for example, [132–136]). Daimler Benz, the parent company of Mercedes-Benz, developed a hydrogen-powered passenger car called NECAR II (New Electric Car) that seats six, has a top speed of 110 km/h (68.4 mph) and a range of 250 km (155 miles) between refueling. It is virtually silent, substantially more energy efficient than even battery-powered

cars and environmentally friendly (releasing water vapor as its only emission). In the fuel cell, oxygen from the air is mixed with hydrogen gas, carried in special cylinders on the roof of the car. A special foil, which forms an electrolyte, separates the two gases and prevents detonation. The process uses a platinum catalyst to strip the electrons from the hydrogen molecule, leaving hydrogen ions. The electrons are allowed to flow through an external circuit from the anode to the cathode, providing work. The hydrogen ions flow through a proton exchange membrane to a second electrode, where they combine with oxygen and the electrons from the cathode to form water. Since heat is generated, the water is discharged as steam. The electricity generated is used to drive an electric motor on the vehicle. Fuel cells are at present extremely expensive to construct, heavy and bulky, but improvements can be expected. Daimler Benz, however, has already presented the new generation NECAR III that is filled up with methanol. With the aid of a reformer located in the rear of the vehicle, this liquid fuel is converted into hydrogen by water-vapor reformation. One can expect these last trends to significantly affect the use of metal hydrides in the automobile industry.

Besides using metal hydrides as a storage media of fuel hydrogen, they can be used to store energy as electrochemical energy in solid solution electrodes. Battery applications center around the so-called nickel-hydrogen battery, a highly reliable rechargeable system first developed for satellite applications [137]. With charging in a sealed cell, a substantial gaseous H_2 pressure results, of as much as 3.5 MPa. The charging pressure can be reduced by using intermetallic H_2 storage compounds, thus reducing pressure vessel requirements and overall cell weight. One method is to simply absorb the H_2 gas product in say a small $LaNi_5$ pellet. The second method is to electrochemically transfer the H produced during charging directly from the KOH electrolyte to an intermetallic storage electrode. The positive electrode in such batteries corresponds to the conventional NiOOH electrode, the negative electrode is supporting the intermetallic hydride. The reactions taking place during discharging can be described by Eq. (9). During the discharging process, trivalent Ni is reduced to divalent Ni while hydrogen is oxidized, involving the decomposition of the hydride. The main advantages of these batteries include high energy density, possibility of high rates of charging/discharging, and low operating temperature of the hydride electrode. The major difficulties are usually concerned with the poor long-term behavior due to surface damage of the hydride electrode, leading to a drastic drop in capacity after a few cycles [128, 129].

$$\begin{aligned} MH_x + xOH^- &\rightarrow M + xH_2O + xe^- && \text{negative hydride electrode (cathode)} \\ NiOOH + H_2O + e^- &\rightarrow Ni(OH)_2 + OH^- && \text{positive Ni electrode (anode)} \\ xNiOOH + MH_x &\rightarrow M + xNi(OH)_2 && \text{overall reaction} \end{aligned} \tag{9}$$

Since the conventional intermetallic hydrides are approaching practical thermodynamic limits, there is a modern tendency to look toward complex hydrides and unconventional alloys, such as nanocrystalline and amorphous ones, as the principal hopes for the future [138]. In the present work we reviewed the properties (e.g., pressure-concentration isotherms, hydrogen capacity, volume change and microstructural stability), which should determine whether amorphous metals and alloys are suitable for hydride device design.

Amorphous alloys may be advantageous for hydrogen storage due to their larger hydrogen capacity, wide composition range, higher corrosion resistance, and localized ductility that should lead to a reduced tendency for disintegration during absorption/desorption cycles. Spit et al. [42, 43], as aforementioned, reported that after a small number of hydriding-dehydriding cycles, no disintegration of amorphous $Ni_{64}Zr_{36}$ samples was observed. However, they refer to the absence of plateau in the pressure-composition isotherms of amorphous alloys, in comparison with equivalent crystalline alloys, as an advantageous characteristic for hydrogen storage applications; they claim it to indicate that no hydride is formed although appreciable amounts of hydrogen can be dissolved in these alloys. Therefore, since plastic deformation that usually accompanies hydride formation is avoided, destruction during cycling will not occur. One should note, on the other hand, that the complete absence of a plateau is usually undesirable for gas-based practical hydride devices like hydrogen storage, where limited charging and discharging pressure ranges are imposed [138]. Yet, the absence of a plateau is not necessarily a barrier to the use of amorphous alloys in batteries [139, 140]. Furthermore, Köster et al. [51] suggest the combinations of various metastable microstructures, with small additions of catalyst, to further improve the storage capacity and hydriding/dehydriding kinetics of Mg-based hydrogen storage alloys.

Disadvantages of amorphous alloys for storage applications also include the often rather small reversibility of hydrogen charging, the need to avoid the crystallization temperature ($T_{\text{cryst}} \sim 300$–$500^{\circ}\text{C}$) during charging, and the possible reduction in thermal stability due to high hydrogen contents [51].

In addition to hydrogen storage, amorphous metals and alloys might also be favorable as hydrogen getters. The growth of fusion technology has resulted in an increasing need for getters especially useful for hydrogen and its isotopes, particularly tritium. Traditionally, the species gettering of hydrogen isotopes has been done with uranium getter beds. However, since amorphous metals are usually considered to be less damaged by radiation [141–143], we can expect them to be better candidates for such applications in nuclear reactors. Other potential applications for amorphous materials include heat pumps and refrigerators [144].

9. Concluding remarks

In this work we have tried to provide a reasonable thorough review of the most important characteristics of hydrogen interaction with amorphous metals and alloys, along with different actual and potential applications. Since this field is relatively young, with only about 20 years of scientific and technological activities, we believe that breakthroughs and development of new applications are not ended yet.

Acknowledgment

Noam Eliaz would like to thank the Israel Ministry of Science for its partial financial support through Eshkol Grant no. 2206-0587 for Scientific Infrastructures.

References

1. H.-J. Güntherodt and H. Beck (eds.), *Glassy Metals I*, Topics in Applied Physics, vol. 46 (Springer-Verlag, Berlin, 1981).
2. H. Beck and H.-J. Güntherodt (eds.), *Glassy Metals II*, Topics in Applied Physics, vol. 53 (Springer-Verlag, Berlin, 1983).
3. F.E. Luborsky (ed.), *Amorphous Metallic Alloys* (Butterworths, London, 1983).
4. S.R. Elliott, *Physics of Amorphous Materials* (Longman Scientific & Technical, New York, 1990).
5. H.H. Liebermann (ed.), *Rapidly Solidified Alloys* (Marcel Dekker, New York, 1993).
6. S. Steeb and H. Warlimont (eds.), *Rapidly Quenched Metals* (Elsevier, Amsterdam, 1985).
7. G. Bambakidis and R.C. Bowman, Jr. (eds.), *Hydrogen in Disordered and Amorphous Alloys* (Plenum, New York, 1986).
8. R.W. Cochrane and J.O. Ström-Olsen (eds.), *Rapidly Quenched Metals* (Elsevier, Amsterdam, 1988).
9. Journal of Non-Crystalline Solids **61/62** (1984).
10. Journal of Non-Crystalline Solids **117/118** (1990).
11. A.J. Maeland, in *Metal Hydrides*, edited by G. Bambakidis (Plenum, New York, 1981), p. 177.
12. A.J. Maeland, in *Rapidly Quenched Metals*, edited by S. Steub and H. Warlimont (Elsevier, Amsterdam, 1985), p. 1507.
13. A.J. Maeland, in *Hydrogen in Disordered and Amorphous Alloys*, edited by G. Bambakidis and R.C. Bowman, Jr. (Plenum, New York, 1986), p. 127.
14. A.J. Maeland, L.E. Tanner, and G.G. Libowitz, Journal of the Less-Common Metals **74**, 279 (1980).
15. K. Suzuki, Journal of the Less-Common Metals **89**, 183 (1983).
16. R.C. Bowman, Jr., Materials Science Forum **31**, 197 (1988).
17. L. Schlapbach (ed.), *Hydrogen in Intermetallic Compounds II*, Topics in Applied Physics, vol. 67 (Springer-Verlag, Berlin, 1992).
18. N. Eliaz and D. Eliezer, Scripta Materialia, to be published.
19. R. Kirchheim, Acta Metallurgica **30**, 1069 (1982).
20. R. Kirchheim, F. Sommer, and G. Schluckebier, Acta Metallurgica **30**, 1059 (1982).
21. R. Kirchheim, Acta Metallurgica **21**, 1233 (1973).
22. R. Kirchheim, T. Mütschele, W. Kieninger, H. Gleiter, R. Birringer, and T.D. Koble, Materials Science and Engineering **99**, 457 (1988).
23. J.H. Harris, W.A. Curtin, and M.A. Tenhover, Physical Review B **36**, 5784 (1987).
24. W.A. Curtin and J.H. Harris, Materials Science and Engineering **99**, 463 (1988).
25. J.H. Harris, W.A. Curtin, and L. Schulz, Journal of Materials Research **3**, 872 (1988).
26. J.H. Harris, W.A. Curtin, and M.A. Tenhover, in *Proc. of the MRS Inter. Meeting on Advanced Materials*, edited by Y. Moro-oka, S. Ono, Y. Sasaki, and S. Suda (MRS, Pittsburgh, vol. 2, 1989), p. 21.
27. J.H. Harris and W.A. Curtin, Zeitschrift für Physikalische Chemie Neue Folge **163**, 315 (1989).
28. M. Kijek, M. Ahmadzadeh, B. Cantor, and R.W. Cahn, Scripta Metallurgica **14**, 1337 (1980).
29. M. Ahmadzadeh and B. Cantor, Journal of Non-Crystalline Solids **43**, 189 (1981).
30. P.M. Richards, Physical Review B **27**, 2059 (1983).
31. H. Kaneko, T. Kajitani, M. Hirabayashi, M. Ueno, and K. Suzuki, Journal of the Less-Common Metals **89**, 237 (1983).
32. K. Suzuki, N. Hayashi, J. Tomizuka, T. Fukunaga, K. Kai, and N. Watanabe, Journal of Non-Crystalline Solids **61/62** (1984), p. 637.
33. Y. Fukai, *The Metal-Hydrogen System*, Materials Science, vol. 21 (Springer-Verlag, Berlin, 1993), p. 57.
34. J.J. Rush, J.M. Rowe, and A.J. Maeland, Journal of Physics F **10**, L283 (1980).
35. D. Richter, R. Hempelmann, and R.C. Bowman, Jr., in *Hydrogen in Intermetallic Compounds II*, Topics in Applied Physics, vol. 67, edited by L. Schlapbach (Springer-Verlag, Berlin, 1992), p. 97.
36. T. Kajitani, H. Kaneko, and M. Hirabayashi, The Science Reports of the Research Institutes, Tôhoku University, Ser. A **29**, 210 (1981).
37. H. Kaneko, T. Kajitani, M. Hirabayashi, M. Ueno, and K. Suzuki, in *Proc. of the 4th Inter. Conf. on Rapidly Quenched Metals*, edited by T. Masumoto and K. Suzuki (Japan Institute of Metals, Sendai, 1982), p. 1605.
38. M. Hirabayashi, H. Kaneko, T. Kajitani, H. Suzuki, and M. Ueno, AIP Conference Proceedings **89**, 87 (1982).

39. A. Williams, J. Eckert, X.L. Yeh, M. Atzmon, and K. Samwer, Journal of Non-Crystalline Solids **61/62**, 643 (1984).
40. J.-J. Lin and T.-P. Perng, Scripta Metallurgica **25**, 1179 (1991).
41. K. Aoki, M. Kamachi, and T. Masumoto, Journal of Non-Crystalline Solids **61/62**, 679 (1984).
42. F.H.M. Spit, J.W. Drijver, and S. Radelaar, Zeitschrift für Physikalische Chemie Neue Folge **116**, 225 (1979).
43. F.H.M. Spit, J.W. Drijver, and S. Radelaar, Scripta Metallurgica **14**, 1071 (1980).
44. K. Aoki, A. Horata, and T. Masumoto, in *Proc. of the 4th Inter. Conf. on Rapidly Quenched Metals*, edited by T. Masumoto and K. Suzuki (Japan Institute of Metals, Sendai, 1982), p. 1649.
45. K. Samwer and W.L. Johnson, Physical Review B **28**, 2907 (1983).
46. H. Peisl, in *Hydrogen in Metals I*, edited by G. Alefeld and J. Völkl (Springer-Verlag, Berlin, 1978), p. 53.
47. U. Stolz, U. Nagorny, and R. Kirchheim, Scripta Metallurgica **18**, 347 (1984).
48. S.M. Lee and J.Y. Lee, Journal of Applied Physics **63**, 4758 (1988).
49. N. Eliaz, D. Eliezer, E. Abramov, and E.J. Lavernia, in *Proc. of the 3rd Pacific Rim Inter. Conf. on Advanced Materials and Processing*, edited by M.A. Imam, R. DeNale, S. Hanada, Z. Zhong, and D.N. Lee, vol. 2 (TMS, Pennsylvania, 1998), p. 2757.
50. A.J. Maeland, in *Hydride for Energy Storage*, edited by A.F. Andersen and A.J. Maeland (Pergamon, Oxford, 1978), p. 447.
51. U. Köster, D. Zander, H. Alves, and T. Spassov, in *Magnesium 97—Proc. of the 1st Israeli Inter. Conf. on Magnesium Science & Technology*, edited by E. Aghion and D. Eliezer (Magnesium Research Institute LTD., Beer-Sheva, 1998), p. 244.
52. R.W. Lin and H.H. Johnson, Journal of Non-Crystalline Solids **51**, 45 (1982).
53. N.R. Quick and H.H. Johnson, Acta Metallurgica **26**, 903 (1978).
54. T.-P. Perng and C.J. Altstetter, Acta Metallurgica **34**, 1771 (1986).
55. E. Abramov, *Synergistic Effects of Hydrogen Isotopes and Helium on Nickel*, Ph.D. Thesis (Ben-Gurion University of the Negev, Beer-Sheva, 1992).
56. J.-J. Lin and T.-P. Perng, Acta Metallurgica **39**, 1101 (1991).
57. J.-J. Lin and T.-P. Perng, Metallurgical and Materials Transactions A **26**, 191 (1995).
58. R.M. Latanision, C.R. Compeau, and M. Kurkela, in *Hydrogen Embrittlement and Stress Corrosion Cracking*, edited by R. Gibala and R.F. Hehemann (ASM, Ohio, 1984), p. 297.
59. M. Hara and R.M. Latanision, Corrosion Science **37**, 865 (1995).
60. J. Flis, S. Ashok, N.S. Stoloff, and D.J. Duquette, Acta Metallurgica **35**, 2071 (1987).
61. B.S. Berry and W.C. Pritchet, Physical Review B **24**, 2299 (1981).
62. Y. Sakamoto and A. Miura, Journal of the Japanese Institute of Metallurgy **42**, 331 (1971).
63. R.W. Cahn, in *Physical Metallurgy*, edited by R.W. Cahn and P. Haasen (North-Holland, Amsterdam, 1983), p. 1780.
64. C. Birac and D. Lesueur, Physica Status Solidi A **36**, 247 (1976).
65. H. Hahn and R.S. Averback, Physical Review B **37**, 6533 (1988).
66. J. Völkl and G. Alefeld, in *Hydrogen in Metals I*, edited by G. Alefeld and J. Völkl (Springer-Verlag, Berlin, 1978), p. 321.
67. R. Kirchheim and U. Stolz, Acta Metallurgica **35**, 281 (1987).
68. Y.S. Lee and D.A. Stevenson, Journal of Non-Crystalline Solids **72**, 249 (1985).
69. K. Aoki, A. Horata, and T. Masumoto, The Science Reports of the Research Institutes, Tôhoku University, Ser. A **29**, 218 (1981).
70. U. Stolz, M. Weller, and R. Kirchheim, Scripta Metallurgy **20**, 1361 (1986).
71. B.S. Berry and W.C. Pritchet, Journal de Physique **45**, C10-457 (1985).
72. B.S. Berry and W.C. Pritchet, in *Nontraditional Methods in Diffusion*, edited by G.E. Murch, H.K. Birnbaum, and J.R. Cost (Metallurgical Society AIME, Warrendale, 1983), p. 83.
73. B.S. Berry and W.C. Pritchet, in *Hydrogen in Disordered and Amorphous Alloys*, edited by G. Bambakidis and R.C. Bowman, Jr. (Plenum, New York, 1986), p. 237.
74. R.C. Bowman, Jr. and A.J. Maeland, Physical Review B **24**, 2328 (1981).
75. R.C. Bowman, Jr., A.J. Maeland, and W.-K. Rhim, Physical Review B **26**, 6362 (1982).
76. R.C. Bowman, Jr., A. Attala, A.J. Maeland, and W.L. Johnson, Solid State Communications **47**, 779 (1983).
77. R. Kirchheim and U. Stolz, Journal of Non-Crystalline Solids **70**, 323 (1985).

78. M. Ahmadzadeh and B. Cantor, in *Proc. of the 4th Inter. Conf. on Rapidly Quenched Metals*, edited by T. Masumoto and K. Suzuki (Japan Institute of Metals, Sendai, 1982), p. 591.
79. J.J. Kimm and D.A. Stevenson, Journal of Non-Crystalline Solids **101**, 187 (1988).
80. J. Shinar, Materials Science Forum **31**, 143 (1988).
81. D. Richter, G. Driesen, R. Hempelmann, and I.S. Anderson, Physical Review Letters **57**, 731 (1986).
82. R. Kirchheim, Progress in Materials Science **32**, 261 (1988).
83. T.T. Markert, E.J. Cotts, and R.M. Cotts, Physical Review B **37**, 6446 (1988).
84. R.C. Bowman, Jr., D.R. Torgeson, R.G. Barnes, A.J. Maeland, and J.J. Rush, Zeitschrift für Physikalische Chemie Neue Folge **163**, 425 (1989).
85. P. Boyer and A. Baudry, Journal of the Less-Common Metals **129**, 213 (1987).
86. A. Chikdene, A. Baudry, and P. Boyer, Journal of Physics F **18**, L187 (1988).
87. A. Chikdene, A. Baudry, and P. Boyer, Zeitschrift für Physikalische Chemie Neue Folge **163**, 443 (1989).
88. J.J. Rush, T.J. Udovic, R. Hemeplmann, D. Richter, and G. Driesen, Journal of Physics: Condensed Matter **1**, 1061 (1989).
89. G. Driesen and K.W. Kehr, Physical Review B **39**, 8132 (1989).
90. N. Eliaz, D. Fuks, and D. Eliezer, Materials Letters, in press.
91. J.S. Cantrell and R.C. Bowman, Jr., Materials Research Society Symposia Proceedings **80**, 105 (1987).
92. J.E. Wagner, R.C. Bowman, Jr., and J.S. Cantrell, Journal of Applied Physics **58**, 4573 (1985).
93. R.C. Bowman, Jr., J.S. Cantrell, E.L. Venturini, R. Schulz, J.E. Wagner, A. Attalla, and B.D. Craft, in *Rapidly Quenched Metals*, edited by S. Staeb and H. Warlimont (Elsevier, Amsterdam, 1985), p. 1541.
94. X.L. Yeh and E.J. Cotts, Journal of Materials Research **2**, 173 (1987).
95. K. Dini and R.A. Dunlap, Journal of Physics F **15**, 273 (1985).
96. S.M. Fries, H.G. Wagner, S.J. Campbell, U. Gonser, N. Blaes, and P. Steiner, Journal of Physics F **15**, 1179 (1985).
97. R.C. Bowman, Jr., R.J. Furlan, J.S. Cantrell, and A.J. Maeland, Journal of Applied Physics **56**, 3362 (1984).
98. R.J. Furlan, G. Bambakidis, J.S. Cantrell, R.C. Bowman, Jr., and A.J. Maeland, Journal of the Less-Common Metals **116**, 375 (1986).
99. R.A. Dunlap and K. Dini, Journal of Physics F **14**, 2797 (1984).
100. L. Novák, É. Kisdi-Koszó, and P. Duhaj, in *Proc. of the 9th Inter. Conf. on Rapidly Quenched & Metastable Materials*, edited by P. Duhaj, P. Mrafko and P. Švec (Elsevier, Netherlands, supplement volume, 1997), p. 216.
101. J. Garaguly, A. Lovas, Á. Cziráki, M. Reybold, J. Takács, and K. Wetzig, in *Proc. of the 9th Inter. Conf. on Rapidly Quenched & Metastable Materials*, edited by P. Duhaj, P. Mrafko, and P. Švec (Elsevier, Netherlands, 1997), p. 938.
102. T. Katona, Á. Molnár, and M. Bartók, Materials Science and Engineering A **181**/**182**, 1095 (1994).
103. Á. Molnár, T. Katona, M. Bartók, and K. Varga, Journal of Molecular Catalysis **64**, 41 (1991).
104. Á. Molnár, T. Katona, M. Bartók, I.V. Perczel, Z. Hegedus, and Cs. Kopasz, Materials Science and Engineering A **134**, 1083 (1991).
105. T. Katona, Á. Molnár, M. Varga, and A. Lovas, in *Proc. of the 9th Inter. Conf. on Rapidly Quenched & Metastable Materials*, edited by P. Duhaj, P. Mrafko, and P. Švec (Elsevier, Netherlands, supplement volume, 1997), p. 380.
106. M. Lazarova, T. Spassov, and S. Budurov, International Journal of Rapidly Solidification **8**, 133 (1994).
107. T. Spassov and G. Tzolova, Crystallization Research Technology **29**, 99 (1994).
108. D. Zander, H. Leptien, U. Köster, N. Eliaz, and D. Eliezer, Journal of Non-Crystalline Solids, in press.
109. D. Menzel, A. Niklas, and U. Köster, Materials Science and Engineering A **133**, 312 (1991).
110. A.S. Tetelman and W.D. Robertson, Transactions AIME **224**, 775 (1962).
111. N.J. Petch and P. Stables, Nature **169**, 842 (1952).
112. W.J. Barnett and A.R. Troiano, Metallurgical Transactions AIME **209**, 486 (1957).
113. J.K. Tien, A.W. Thompson, I.M. Bernstein, and R.J. Richards, Metallurgical Transactions A **7**, 821 (1976).
114. P. Bastien and P. Azou, in *Proceedings of the World Metallurgy Congress* (First American Society of Metals, 1951), p. 535.
115. A.N. Stroh, Advances in Physics **6**, 418 (1957).
116. C.D. Beachem, Metallurgical Transactions **3**, 437 (1972).

117. D.S. Shih, I.M. Robertson, and H.K. Birnbaum, Acta Metallurgica **36**, 111 (1988).
118. D.G. Westlake, Transactions ASM **62**, 1000 (1969).
119. H.K. Birnbaum, in *Hydrogen Effects on Material Behavior*, edited by N.R. Moody and A.W. Thompson (The Minerals, Metals & Materials Society, Warrendale, 1990), p. 639.
120. J.-J. Lin and T.-P. Perng, Metallurgical and Materials Transactions A **26**, 197 (1995).
121. J.-J. Lin and T.-P. Perng, Journal of Materials Science Letters **10**, 1443 (1991).
122. T.K. Namboodhiri, T.A. Ramesh, G. Singh, and S. Seghal, Materials Science and Engineering **61**, 23 (1983).
123. S. Takayama and R. Maddin, Materials Science and Engineering **23**, 261 (1976).
124. S. Ashok, N.S. Stoloff, M.E. Glicksman, and T. Slavin, Scripta Metallurgica **15**, 331 (1981).
125. A. Kawashima, K. Hashimoto, and T. Masumoto, Scripta Metallurgica **14**, 41 (1980).
126. H.W. Schroeder and U. Köster, Journal of Non-Crystalline Solids **56**, 213 (1983).
127. N. Eliaz, D. Eliezer, E. Moshe, and S. Eliezer, to be published.
128. G. Sandrock, S. Suda, and L. Schlapbach, *Hydrogen in Intermetallic Compounds II*, Topics in Applied Physics, vol. 67 (Springer-Verlag, Berlin, 1992), p. 197.
129. P. Dantzer, in *Hydrogen in Metals III*, Topics in Applied Physics, vol. 73, edited by H. Wipf (Springer-Verlag, Berlin, 1997), p. 279.
130. K.E. Cox, in *Effect of Hydrogen on Behavior of Materials*, edited by A.W. Thompson and I.M. Bernstein (The Metallurgical Society of AIME, New York, 1976), p. 3.
131. R.E. Billings, in *Effect of Hydrogen on Behavior of Materials*, edited by A.W. Thompson and I.M. Bernstein (The Metallurgical Society of AIME, New York, 1976), p. 18.
132. http://www.mercedes-benz.co.uk/pr230596b.htm
133. http://194.221.235.100/e/cars/a-class/facts4.htm
134. http://www.eece.ksu.edu/∼ehflora/eece581/H2Fuel.html
135. http://members.australis.net.au/∼engineer/ew/04cars.html
136. http://www.cartoday.com/content/newtec53.shtml
137. M. Klein and B.S. Baker, in *Proc. of the 9th Intersociety Energy Conversion Engineering Conf.* (American Society of Mechanical Engineering, New York, 1974), p. 118.
138. G. Sandrock and M.A. Imam, in *Proc. of the 3rd Pacific Rim Inter. Conf. on Advanced Materials and Processing*, edited by M.A. Imam, R. DeNale, S. Hanada, Z. Zhong, and D.N. Lee, vol. 1 (TMS, Pennsylvania, 1998), p. 601.
139. K. Sapru, A.R. Reichman, and S.R. Ovshinsky, US Patent 4-623-597, November 18 (1986).
140. D.H. Ryan, F. Dumias, B. Patel, J. Kycia, and J.O. Ström-Olsen, Journal of the Less-Common Metals **172–174**, 1246 (1991).
141. R. Mishra and V. Singh, Radiation Effects and Defects in Solids **128**, 315 (1994).
142. S. Klaumünzer, G. Schumacher, S. Rentzsch, G. Vogl, L. Söldner, and H. Bieger, Acta Metallurgica **30**, 1493 (1982).
143. E.A. Kramer, W.L. Johnson, and C. Cline, Applied Physics Letters **35**, 815 (1979).
144. F.H.M Spit, K. Blok, E. Hendriks, G. Winkels, W. Turkenberg, J.W. Drijver, and S. Radelaar, in *Proc. of the 4th Inter. Conf. on Rapidly Quenched Metals*, edited by T. Masumoto and K. Suzuki (Japan Institute of Metals, Sendai, 1982), p. 1635.